# Examination of the Charge-Sensitive Vibrational Modes in Bis(ethylenedithio)tetrathiafulvalene

**Takashi Yamamoto,*,† Mikio Uruichi,† Kaoru Yamamoto,† Kyuya Yakushi,† Atushi Kawamoto,‡ and Hiromi Taniguchi§**

*Institute for Molecular Science, Myodaiji, Okazaki 444-8585, Japan, Department of Physics, Hokkaido University, Kita-ku, Sapporo 060-0810, Japan, and Department of Physics, Saitama University, Sakura-ku, Saitama 338-8570, Japan*

*Received: January 14, 2005; In Final Form: May 2, 2005*

We reinvestigated the two C═C stretching modes of the five-membered rings of ET (ET = bis(ethylenedithio)-tetrathiafulvalene), namely, $\nu_2$ (in-phase mode) and $\nu_{27}$ (out-of-phase mode). The frequency of the $\nu_{27}$ mode of $ET^+$ was corrected to be ~1400 $cm^{-1}$, which was identified from the polarized infrared reflectance spectra of $(ET)(ClO_4)$, $(ET)(AuBr_2Cl_2)$, and the deuterium- or $^{13}C$-substituted compounds of $(ET)(AuBr_2Cl_2)$. It was clarified from DFT calculations that the frequency of the $\nu_{27}$ mode of the flat $ET^0$ molecule was significantly different from that of the boat-shaped $ET^0$ molecule. We obtained the linear relationship between the frequency and the charge on the molecule, $\rho$, for the flat ET molecule, which was shown to be $\nu_{27}(\rho) = 1398 + 140(1 - \rho)$ $cm^{-1}$. The frequency shift due to oxidation is remarkably larger than that reported in previous studies. The fractional charges of several ET salts in a charge-ordered state can be successfully estimated by applying this relationship. Therefore, the $\nu_{27}$ mode is an efficient probe to detect $\rho$ in the charge-transfer salts of ET. Similarly, a linear relationship for the $\nu_2$ mode was obtained as $\nu_2(\rho) = 1447 + 120(1 - \rho)$. This relationship was successfully applied to the charge-poor molecule of $\theta$-type ET salts in the charge-ordered state but could not be applied to the charge-rich molecule. This discrepancy was semiquantitatively explained by the hybridization between the $\nu_2$ and $\nu_3$ modes.

## I. Introduction

Charge-transfer salts containing ET (bis(ethylenedithio)-tetrathiafulvalene) have yielded various compounds, including stable metallic compounds, metallic compounds having a metal−insulator transition or superconducting transition, and semiconducting compounds.[1] In highly conducting ET salts, the molecules form two-dimensional sheets, which are separated from each other by an anion layer. The arrangement of ET molecules in the form of two-dimensional sheets is classified into various groups represented by Greek letters.[2] The metal−insulator transitions of several α-, $\beta''$-, and $\theta$-type ET salts have been characterized as the charge-ordering (CO) phase transition.[3−7] The CO phase transition originates from the localization of charge due to on-site and intersite Coulombic interactions. The representative CO state is the "horizontal stripe", shown in Figure 1, where the charge-rich and -poor molecules are accommodated in the two-dimensional layer.[8] The charge ordering is a current subject in solid-state physics that is related to superconductivity,[9,10] ferroelectricity,[11] unusual electron dynamics,[12] etc. The CO state has been studied by means of broad-band NMR,[13] X-ray diffraction,[14] and vibrational spectroscopy,[3−7] which complement each other. The fractional charge on the ET molecule in the CO state has been detected from the frequency of the Raman-active mode, $\nu_2$, which has a linear relationship between the frequency and the charge on the molecule.[15] As shown in Figure 2, the $\nu_2$ mode is the in-phase stretching mode of the C═C bonds in two five-membered rings of ET. Recently, the insulator−superconductor transition is attracting attention in several ET salts, since the CO state is predicted to be neighbored to a new type of superconducting state.[9] To study the CO state near the superconductivity, Raman spectroscopy is not always useful because of the heating effect of the excitation laser. In this sense, the detection of the infrared-active C═C stretching mode is indispensable.

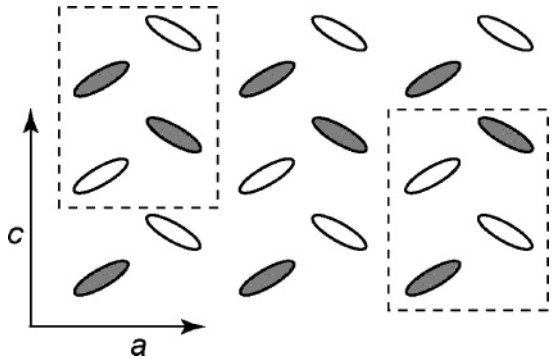


**Figure 1.** Schematic views of the "horizontal stripe" viewed along the molecular long axis. A gray (opened) ellipse denotes the charge-rich (poor) molecule. Broken lines denote the nonlinear tetramer shown at the corners of Figure 8.

The infrared-active mode paired with the $\nu_2$ mode is the $\nu_{27}$ mode, which is the out-of-phase stretching mode of the C═C bond in the five-membered rings of ET (Figure 2). The transition

* To whom correspondence should be addressed. E-mail: yamataka@ims.ac.jp. Tel: +81-564-55-7382. Fax: +81-564-54-2254.
† Institute for Molecular Science.
‡ Hokkaido University.
§ Saitama University.

10.1021/jp050247o CCC: $30.25 
Published on Web 07/21/2005

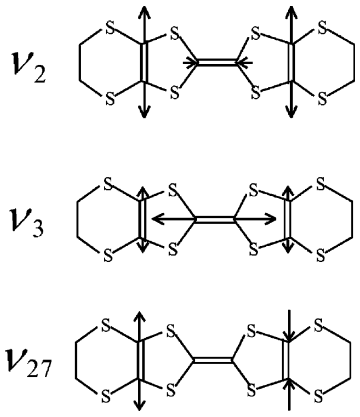


**Figure 2.** Schematic views of the three fundamental C═C stretching modes of the ET molecule.

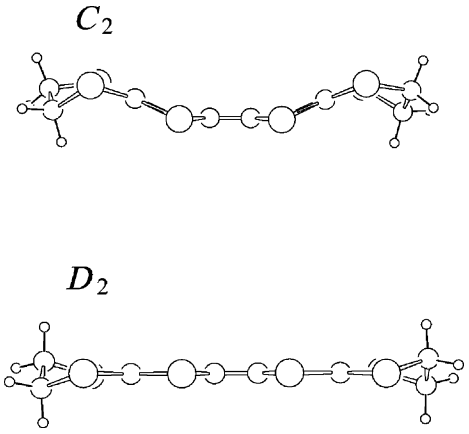


**Figure 3.** The ET molecular structures of the boat ($C_2$ symmetry) and flat ($D_2$ symmetry) molecules.

dipole of this mode is polarized along the long molecular axis of ET, which is perpendicular to the conducting sheet. Because of this geometrical configuration, we can avoid strong electronic absorption and can detect a clear vibrational band if we use light that is polarized perpendicular to the conducting sheet. Furthermore, the $\nu_{27}$ mode is not perturbed by the e-mv (electron-molecular vibration) interaction which sometimes has a big influence on the frequency of the $\nu_3$ mode.[16] Therefore, the observation of the $\nu_{27}$ mode is more appropriate for the estimation of the fractional charge, especially at low temperatures, if the side face of the single crystal is large enough.

The liner relationship between the fractional charge and the frequency of the $\nu_{27}$ mode was presented by J. Moldenhauer et al.[17] based on the assignment of $ET^0$ and $ET^+$ by Kozlov et al.[18,19] According to their analyses, the frequency of the $\nu_{27}$ mode is $\sim$1509 $cm^{-1}$ for $ET^0$ and $\sim$1445 $cm^{-1}$ for $ET^+$. However, the frequency of the infrared-active C═C stretching band of the neutral-like (cationic) ET molecule in the CO state is sometimes higher (lower) than $\sim$1509 $cm^{-1}$ ($\sim$1445 $cm^{-1}$).[4] We surmise that the inconsistency is ascribed to the incorrect assignment for the powder spectrum of $ET^+$ compounds. In this paper, we will give the new assignment of the $\nu_{27}$ of $ET^+$ based on the polarized infrared and the Raman spectra using the side face of the single crystal of the CT salts represented as $ET^+A^-$ ($A^-$, anion). Compared with the assignment of $\nu_{27}$ of $ET^+$, the assignment of $\nu_{27}$ ($\sim$1509 $cm^{-1}$) of $ET^0$ is much more reliable.[18,20,21] As shown in Figure 3, the molecule at the charge-poor site maintains a planar structure except for the ethylene end groups ($D_2$ symmetry),[14] whereas the $ET^0$ in the neutral crystal has a boat structure ($C_2$ symmetry).[22] Since the nearly neutral molecule in a CO state has a planar structure, we examined the structural dependence of the frequency of the $\nu_{27}$ ($\nu_2$) mode using the density functional theory (DFT) method. Through the experiments and calculations, we will give the reliable relationship between the frequency of $\nu_{27}$ and the fractional charge of the ET molecule, which is significantly different from the relationship deduced from the previous reports.[17−19]

This paper is organized as follows. In section II, we describe the experimental and computational procedures used in the study. In section III-A, we examine the polarized infrared and Raman spectra of the single crystals of several $ET^+$ compounds. In section III-B, we show the calculation of the normal modes of the flat and boat $ET^0$. In section III-C, we demonstrate the linear relationship between the frequency of $\nu_{27}$ and the fractional charge of the ET molecule. The validity of the liner relationship is examined using the vibrational spectra in the CO state of several CT salts. Finally, in section III-D, we show examples for which the frequency of $\nu_2$ deviates from the linear relationship and discuss the reasons for this deviation from the standpoint of the hybridization between the $\nu_2$ mode and the $\nu_3$ mode perturbed by the e-mv interaction.

## II. Experimental and Computational Procedures

Single crystals containing ET and $ClO_4$ were obtained from a mixture of ET and tetrabutylammonium perchlorate (TBA($ClO_4$)) dissolved in 1,1,2-trichloroethane (TCE) using the electrocrystallization method. (ET)($ClO_4$) was harvested as a minor product, while the major products were $\beta''$-$(ET)_3(ClO_4)_2$ and $\beta''$-$(ET)_2(ClO_4)$TCE. The (ET)($ClO_4$) salt was also obtained by electrocrystallization from a dichloromethane ($CH_2Cl_2$) solution of ET and TBA($ClO_4$).[23] In this case also, (ET)($ClO_4$) was a minor product, while the main phase was $\beta''$-$(ET)_3(ClO_4)_2$. (ET)($ClO_4$) was identified as the same compound reported earlier by Abboud et al.[24] using X-ray crystal structure analysis. The crystal habit of (ET)($ClO_4$) was a thick black plate, easily distinguishable from the thin plate crystals of $\beta''$-$(ET)_3(ClO_4)_2$ and $\beta''$-$(ET)_2(ClO_4)$TCE. Three single crystals were also distinguished from one another through measurements of the reflectance and the Raman spectra.

Single crystals of (ET)($AuBr_2Cl_2$) were grown through electrocrystallization of a mixture of ET and TBA($AuBr_2Cl_2$) dissolved in $CH_2Cl_2$. The supporting electrolyte, TBA-($AuBr_2Cl_2$), was synthesized by refluxing the acetonitrile solution of TBA[$Au^{III}Cl_4$] and (TBA)Br. The main product was (ET)($AuBr_2Cl_2$). (ET)($AuBr_2Cl_2$) was identified as the same compound reported by Porter et al.[25] using X-ray crystal structure analysis. The crystal habit of the main product was a thin black plate, and that of the minor product was a rectangular needle. Two modifications were also distinguished from each other by using reflectance or Raman spectrum. The isotope analogues of (ET)($AuBr_2Cl_2$) were synthesized using the same procedure as for the normal compound. The isotope substitutions were applied to all the hydrogen atoms in the ethylenedithio end groups of ET, or to the central C═C carbons of ET. Hereafter, the former is expressed as ($d_8$-ET)($AuBr_2Cl_2$), the latter as ($^{13}$C-ET)($AuBr_2Cl_2$), and the normal compound as (ET)($AuBr_2Cl_2$).

Polarized reflectance spectra were obtained using a Nicolet Magna 760 FT-IR spectrometer combined with a Spectratech IR-Plan microscope. The spectral resolution was 4 $cm^{-1}$. The light polarization was parallel to the stacking direction in the two-dimensional (2-D) sheet or almost parallel to the long axis of the ET molecule. We collected a reflectance spectrum by

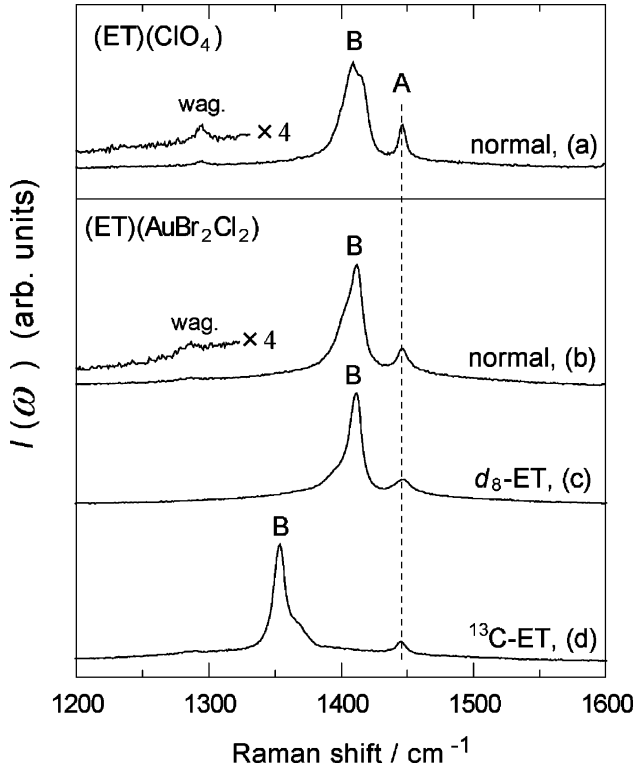


**Figure 4.** Raman spectra of (a) $(ET)(ClO_4)$, (b) $(ET)(AuBr_2Cl_2)$, (c) $(d_8\text{-}ET)(AuBr_2Cl_2)$, and (d) $(^{13}C\text{-}ET)(AuBr_2Cl_2)$ excited by a 780 nm laser.

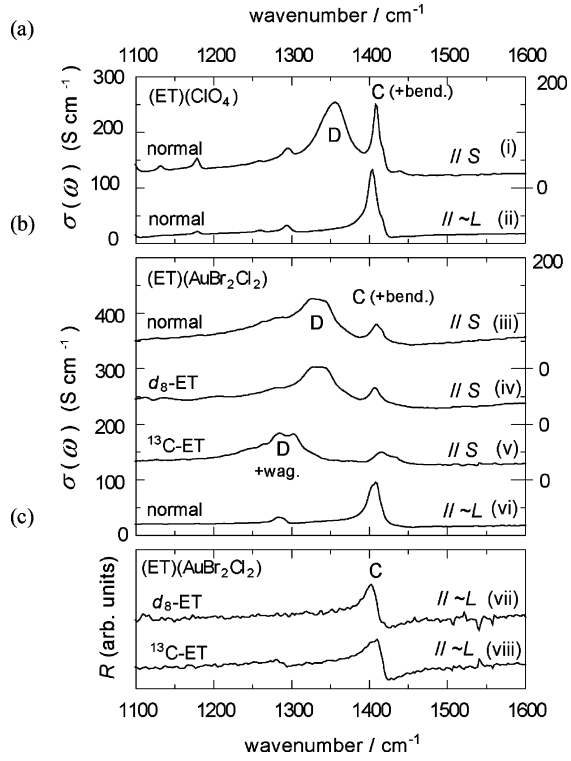


**Figure 5.** (a) Optical conductivity spectra of $(ET)(ClO_4)$. (b) Optical conductivity spectra of $(ET)(AuBr_2Cl_2)$ and isotope analogues. (c) Reflectance spectra of the isotope analogues of $(ET)(AuBr_2Cl_2)$. The conductivity spectra, denoted as "// S", are obtained from the reflectance spectra measured with the light polarized along the stacking direction. "// ~L" denotes the experimental condition, where the polarization of the incident light is almost parallel to the long axis of the ET molecule.

accumulating 256 scans. This procedure was repeated four times, so that the total number of scans reached 1024 scans. The resulting spectrum was thus obtained after averaging four spectra. To obtain the conductivity spectra, we measured the reflectance spectra from 600 $cm^{-1}$ up to 12 000 $cm^{-1}$. Raman spectra were measured using a Renishaw Raman microscope system in the backward-scattering configuration. The sample was irradiated by a 780 nm laser. The intensity of the excitation light was reduced below 0.1 mW to avoid radiation damage. Although the incident light was polarized, no polarizer was applied to the scattered light. The spectral resolution was 2 $cm^{-1}$. Frequency corrections to the observed Raman shift were made using the TO mode of diamond (1332 $cm^{-1}$) and a Ne lamp. All spectra were collected at 300 K.

Quantum chemical calculations were performed with the Gaussian 98 program.[26] Geometrical optimizations were conducted using the DFT (B3LYP) method using standard 6-31G** basis sets.[27] Geometrical optimization for the $ET^0$ was conducted assuming $C_2$ symmetry for the boat structure and $D_2$ symmetry for the flat structure. Figure 3 shows the molecular structures of the boat and flat ET, obtained by the geometrical optimization. The most stable structure of the neutral ET is the boat structure ($C_2$), which was in agreement with that obtained by the HF method,[21] whereas the flat structure ($D_2$) was located at the saddle point on the energy surface. The geometrical optimization for the $ET^+$ was conducted assuming the flat structure ($D_2$), which turned out to be the most stable. The frequency calculation was carried out for the optimized structures obtained using the DFT method. The normal modes are classified as $37a + 35b$ for the $C_2$ symmetry, $(19a + 18b_3) + (17b_1 + 18b_2)$ for the $D_2$ symmetry, and $(12a_g + 7a_u) + (11b_{3g} + 7b_{3u}) + (6b_{1g} + 11b_{1u}) + (7b_{2g} + 11b_{2u})$ for the $D_{2h}$ symmetry. Although the numbering of the normal mode depends on the symmetry, we followed the numbering used by Kozlov et al.[18,19] who conducted the normal-mode analysis assuming $D_{2h}$ symmetry. The C═C stretching modes, $\nu_2$, $\nu_3$, and $\nu_{27}$, are shown in Figure 2.

## III. Results and Discussions

**A. Assignments of the C═C Stretching Modes of $ET^+$.** Figure 4 shows the Raman spectra for (a) $(ET)(ClO_4)$, (b) $(ET)(AuBr_2Cl_2)$, (c) $(d_8\text{-}ET)(AuBr_2Cl_2)$, and (d) $(^{13}C\text{-}ET)$-$(AuBr_2Cl_2)$. The excitation light was polarized along the *a*-axis for the $ClO_4$ salt and along the *b*-axis for the $AuBr_2Cl_2$ salts. These polarization directions are almost parallel to the molecular long axis.[28] Figure 5 shows the optical conductivity spectra and reflectance spectra for the $ClO_4$ and $AuBr_2Cl_2$ salts. The symbol "$\sim L$" denotes spectra measured with the *a*-polarized (for the $ClO_4$ salt) and *b*-polarized (for the $AuBr_2Cl_2$ salts) light. The symbol "*S*" denotes spectra measured with the light polarized along the stacking direction. In this spectral region, the observed bands can be assigned to the C═C stretching and $CH_2$-bending modes.

As shown in Figure 4, the A band observed at 1445 $cm^{-1}$ shows no isotope shift in the spectra for the deuterium- and $^{13}C$-substituted compounds. Therefore, the A band is neither the $CH_2$-bending mode nor the $\nu_3$ mode, but it is either the $\nu_2$ or the $\nu_{27}$ mode. Since the ET molecule of these compounds has a flat structure except for the ethylene end groups, the tetrathiafulvalene (TTF) skeleton has a pseudoinversion symmetry. Therefore, it is expected from the mutual exclusion rule that $\nu_2$ is Raman active and $\nu_{27}$ is infrared active. As shown in Figure 5, no vibrational band is observed around the region of 1445 $cm^{-1}$ in the infrared spectra. Therefore, the A band was assigned to the $\nu_2$ mode of $ET^+$.

**TABLE 1: Assignments of the C═C Stretching Modes of (ET)($ClO_4$), (ET)($AuBr_2Cl_2$), ($d_8$-ET)($AuBr_2Cl_2$), and ($^{13}$C-ET)($AuBr_2Cl_2$)**

| band | A ($cm^{-1}$) | B ($cm^{-1}$) | C ($cm^{-1}$) | D ($cm^{-1}$) |
|---|---|---|---|---|
| (ET)($ClO_4$) | 1445 | 1415 | 1400 | ∼1350 |
| (ET)($AuBr_2Cl_2$) | 1445 | 1415 | 1400 | ∼1330 |
| ($d_8$-ET)($AuBr_2Cl_2$) | 1445 | 1415 | 1400 | ∼1330 |
| ($^{13}$C-ET)($AuBr_2Cl_2$) | 1445 | 1355 | 1400 | ∼1280 |
| assignments | $\nu_2$ | $\nu_3$ | $\nu_{27}$ | $\nu_3$ (*e-mv*) |

The B band observed at ∼1415 $cm^{-1}$ in the Raman spectra of the normal compounds in spectra a and b of Figure 4 shows no isotope shift for the deuterium analogue, as can be seen in Figure 4c. On the other hand, the frequency of the B band of the $^{13}$C analogue was lowered to ∼1355 $cm^{-1}$ as shown in Figure 4d. The observed isotope shift from the normal compound is ∼ −4.2% (∼ −60 $cm^{-1}$). This value is very close to $1 - (^{13}/_{12})^{1/2} \sim -4.1\%$, which is expected if the B band is due to the central C═C stretching mode. As shown in spectra v and viii of Figure5, the B band of the $^{13}$C analogue is not observed around 1355 $cm^{-1}$. Therefore, the B band is assigned to the central C═C stretching mode, $\nu_3$, which is Raman active in the $D_{2h}$ symmetry.

As shown in Figure 5, the C band observed around 1400 $cm^{-1}$ in the infrared spectra of $ClO_4$ and $AuBr_2Cl_2$ salts is polarized along the molecular long axis without an isotope shift for both $d_8$- and $^{13}$C-substituted compounds. The corresponding band is not found at the same frequency in the Raman spectrum of ($^{13}$C-ET)($AuBr_2Cl_2$) (Figure 4d). Therefore, the C band is assigned to the out-of-phase stretching mode ($\nu_{27}$) of the wing C═C bonds. Although $\nu_{27}$ should be polarized along the molecular long axis, the C band is also found in all the *S*-polarized spectra of $ClO_4$ and $AuBr_2Cl_2$ salts as shown in Figure 5. This observation is ascribed to the crystal structure wherein the molecular long axis is not perpendicular to the stacking axis but has an angle of 78° in (ET)($AuBr_2Cl_2$) and 37° in (ET)($ClO_4$) with respect to the stacking direction.[24,25]

As shown in the spectra of the normal compounds (Figures 4a, 4b, 5i−iii, and 5vi), the B and C bands have an asymmetric shape, which suggests the presence of an additional band in the region of the B or C band. The additional band is ascribed to the $CH_2$-bending mode, because the deuterium-substituted compound exhibits a symmetric single peak (Figures 4c and 5iv).

In the *S*-polarized infrared spectrum of (ET)($AuBr_2Cl_2$) and ($d_8$-ET)($AuBr_2Cl_2$), the broad and strong band is observed at ∼1330 $cm^{-1}$. The main component of the broad band shows the frequency shift down to ∼1280 $cm^{-1}$ for ($^{13}$C-ET)-($AuBr_2Cl_2$). The isotope shift of the main component, ∼ −3.8% (∼ −50 $cm^{-1}$), roughly agrees with $1 - (^{13}/_{12})^{1/2} \sim -4.1\%$. Therefore, the main component of the broad band is assigned to another $\nu_3$ mode, the D band. The D band of (ET)($ClO_4$) observed at ∼1350 $cm^{-1}$ is slightly higher than that of (ET)($AuBr_2Cl_2$). In both compounds, the D band is located at a lower frequency than the B band ($\nu_3$ mode), and it appears in the *S*-polarized spectrum with a broad line width. In addition, the frequency of the D band depends on the compound. These properties are in agreement with that fact that the D band is assigned to the vibronic $\nu_3$ mode whose frequency is perturbed by the e-mv interaction. Since the e-mv mode is coupled with the CT transition, the D band has a very broad line width, so that the other modes, such as the $CH_2$-wagging mode, are superimposed with the D band. The appearance of the vibronic $\nu_3$ mode is also consistent with the dimerized stack structure in the $ClO_4$ and $AuBr_2Cl_2$ salts,[24,25] because the D band is the off-phase mode between the neighboring molecules within a dimer.

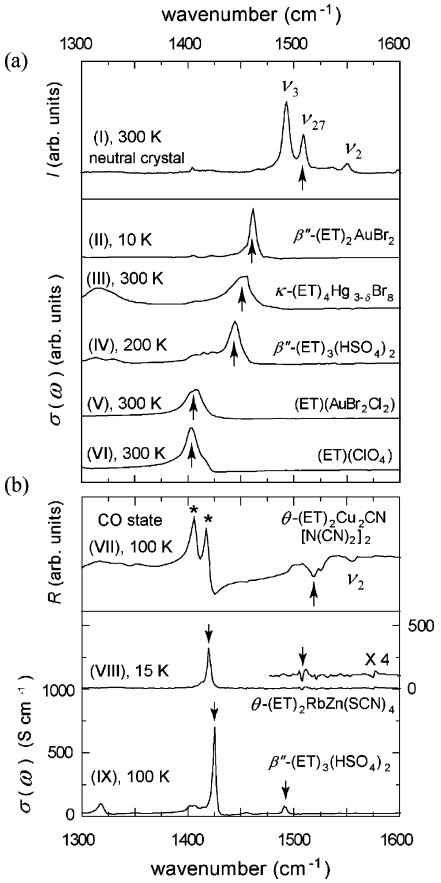


**Figure 6.** (a) Raman spectra of the neutral ET crystal (I) and conductivity spectra of the ET salts II−VI, where the charge of ET, $\rho$, is almost homogeneous. (b) VII: IR reflectance spectra of $\theta$-$(ET)_2Cu_2CN[N(CN)_2]_2$ in the charge-ordered (CO) state at 100 K. VIII and IX: Conductivity spectra of $\theta$-$(ET)_2RbZn(SCN)_4$ (15 K) and $\beta''$-$(ET)_3(HSO_4)_2$ (100 K) in the CO state, respectively. The arrows denote the $\nu_{27}$ modes, and the asterisks denote the candidates of the $\nu_{27}$ modes.

Table 1 summarizes the new assignments which are different from the conventional assignment.[19] On the basis of the infrared spectra of the powder samples of $ET^+I_3^-$ and $ET^+Br^-$, the infrared bands at ∼1400 $cm^{-1}$ (strong intensity) and ∼1445 $cm^{-1}$ (weak intensity) have been assigned to the vibronic $\nu_2$ mode and the $\nu_{27}$ mode of $ET^+$, respectively. However, it is not straightforward in the powdered sample to draw a distinction between the $\nu_{27}$ mode and the vibronic $\nu_2$ mode. The crucial difference between the infrared-active $\nu_{27}$ mode and the vibronic $\nu_2$ mode is the polarization direction; the $\nu_{27}$ mode is polarized along the molecular long axis, whereas the vibronic $\nu_2$ mode is polarized along the stacking direction. Since the C band at ∼1400 $cm^{-1}$ is polarized along the molecular long axis in (ET)($ClO_4$) and (ET)($AuBr_2Cl_2$), the ∼1400 $cm^{-1}$ band of ref 19 should be assigned to $\nu_{27}$. Therefore, the weak band at ∼1445 $cm^{-1}$ in the infrared spectra of $ET^+Br^-$ and $ET^+I^-$ can be assigned to the vibronic $\nu_2$ mode.

**B. C═C Stretching Modes of Boat and Flat $ET^0$.** The C═C stretching modes of a neutral ET crystal have been used as the standard bands of the neutral molecule ($ET^0$). It is well-known that the molecule in the neutral ET crystal does not have a planar structure but rather has a boat structure.[22] The low symmetry of $ET^0$ actually affects the selection rule of the vibrational spectrum. As shown in the top panel of Figure 6a, the infrared-active $\nu_{27}$ mode is observable at ∼1509 $cm^{-1}$ in

**TABLE 2: Frequencies of the C═C Stretching and $CH_2$-Bending, -Wagging, and -Twisting Modes, Obtained from the Normal Mode Analyses Using the DFT (B3LYP) Method[a]**

| | | $\rho = 0$ $C_2$: boat | | | $\rho = 0$ $D_2$: flat | | | $\rho = +1$ $D_2$: flat | |
|---|---|---|---|---|---|---|---|---|---|
| | | mode | frequency ($cm^{-1}$) | | mode | frequency ($cm^{-1}$) | | mode | frequency ($cm^{-1}$) |
| C═C stretching | $\nu_2$ | *a* | 1554 | $\nu_2$ | *a* | 1570 | $\nu_2$ | *a* | 1449 |
| | $\nu_{27}$ | *b* | 1513 | $\nu_{27}$ | $b_1$ | 1538 | $\nu_{27}$ | $b_1$ | 1396 |
| | $\nu_3$ | *a* | 1506 | $\nu_3$ | *a* | 1523 | $\nu_3$ | *a* | 1398 |
| $CH_2$ bending | | *a* | 1434 | | *a* | 1422 | | *a* | 1421 |
| | | *b* | 1434 | | $b_1$ | 1422 | | $b_1$ | 1421 |
| | | *a* | 1412 | | $b_3$ | 1418 | | $b_3$ | 1417 |
| | | *b* | 1412 | | $b_2$ | 1418 | | $b_2$ | 1417 |
| $CH_2$ wagging | | *a* | 1284 | | *a* | 1283 | | *a* | 1287 |
| | | *b* | 1284 | | $b_1$ | 1283 | | $b_1$ | 1285 |
| | | *a* | 1249 | | $b_3$ | 1256 | | $b_3$ | 1260 |
| | | *b* | 1249 | | $b_2$ | 1256 | | $b_2$ | 1259 |
| $CH_2$ twisting | | *a* | 1154 | | *a* | 1164 | | *a* | 1171 |
| | | *b* | 1154 | | $b_1$ | 1164 | | $b_1$ | 1171 |
| | | *a* | 1110 | | $b_3$ | 1111 | | $b_3$ | 1114 |
| | | *b* | 1110 | | $b_2$ | 1111 | | $b_2$ | 1114 |

[a] The scaling factor is 96.14%[30].

the Raman spectrum of the neutral ET crystal.[29] On the other hand, the ET molecules in the CO state have a flat structure with a pseudoinversion center, although the unit cell in the CO state involves not only charge-rich (nearly cationic) but also charge-poor (nearly neutral) molecules.[3,14] We can examine whether the frequency of the C═C stretching modes of the neutral ET crystal can be utilized for the estimation of the charge on each molecule in the CO state. The spectrum of the neutral ET crystal can be compared with that of $\theta$-$(ET)_2Cu_2CN[N(CN)_2]_2$ in the CO state. According to our previous report,[4] the $\nu_{27}$ mode appears as two split bands in the CO state (100 K). The reflectance spectrum is reproduced in the top panel of Figure 6b. Yamamoto et al. assigned one of the peaks marked by asterisks to the $\nu_{27}$ mode in a charge-rich molecule, and he assigned the dip at ~1520 $cm^{-1}$ marked by an arrow to the $\nu_{27}$ mode in a charge-poor molecule.[4] If this assignment is correct, the charge-poor molecule should have a negative charge, because the frequency of $\nu_{27}$ is higher than that in the neutral ET crystal, ~1509 $cm^{-1}$. The $\nu_2$ modes of $\theta$-$(ET)_2Cu_2CN[N(CN)_2]_2$ in the CO state are definitely assigned in the Raman spectrum,[4] and the frequency of the $\nu_2$ mode at the charge-poor site is reported to be ~1550 $cm^{-1}$. This frequency is comparable to that of the $\nu_2$ mode of the neutral ET crystal, ~1550 $cm^{-1}$. Since a negative charge is unreasonable, we consider that the $\nu_2$ and $\nu_{27}$ modes of flat $ET^0$ might have higher frequencies than those of the boat $ET^0$. If this hypothesis is valid, the frequencies of the $\nu_2$ and $\nu_{27}$ modes observed at the charge-poor site become lower than those of the flat $ET^0$, so that the charge-poor molecule has a slightly positive charge.

To verify our conjecture, we calculated the normal modes of the flat and boat $ET^0$ using a DFT (B3LYP) method. $D_2$ and $C_2$ symmetry was, respectively, assumed for the flat and boat structures. Table 2 shows the scaled frequencies of the $\nu_2$, $\nu_3$, and $\nu_{27}$ modes along with the frequencies of the $CH_2$-bending, -wagging, and -twisting modes. The scaled frequencies of the flat $ET^+$ are also shown in Table 2. We adopted a scaling factor of 96.14% which has been recommended by Scott et al.[30] As shown in Table 2, the frequencies of the $\nu_2$, $\nu_3$, and $\nu_{27}$ modes of the $D_2$ symmetry were calculated to be significantly higher than those of the $C_2$ symmetry as we had anticipated.

To the best of our knowledge, there is no compound containing flat ET whose molecular charge is exactly zero. If the frequency calculated for the boat $ET^0$ and flat $ET^+$ quantitatively agrees with the experimentally observed values, then the calculation for the flat $ET^0$ is considered to be quantitatively reliable. The scaled frequencies of the $\nu_2$ and $\nu_{27}$ modes for the boat $ET^0$ are 1554 and 1513 $cm^{-1}$, respectively, which are in good agreement with the observed frequencies of ~1550 ($\nu_2$) and ~1509 $cm^{-1}$ ($\nu_{27}$) for the neutral crystal. As for the flat $ET^+$ (Tables 1 and 2), the deviations of the scaled frequencies from the experimental results are ~ +4 and ~ +4 $cm^{-1}$ for the $\nu_2$ and $\nu_{27}$ modes, respectively. The deviation of the scaled frequencies of $\nu_3$ from the experimental values are ~ +13 and ~ −17 $cm^{-1}$ for the boat $ET^0$ and flat $ET^+$, respectively. The discrepancy in the $\nu_3$ mode of ~1.3% is slightly larger than that of the $\nu_2$ and $\nu_{27}$ modes but is not significantly different. Among several $CH_2$ modes, the A mode of the $CH_2$-wagging mode is actually observed in the Raman spectra. As shown in Figure 4, the $CH_2$-wagging mode is observed at ~1284 and 1294 $cm^{-1}$ in $(ET)(ClO_4)$ and $(ET)(AuBr_2Cl_2)$, respectively. These observations are consistent with the scaled frequency of the flat $ET^+$ of 1287 $cm^{-1}$ within an error of ~0.5%. As for the neutral ET crystal, this mode is observed at 1283 $cm^{-1}$, which is in agreement with the scaled frequency of the boat $ET^0$, 1284 $cm^{-1}$. As shown above, the agreement between the scaled frequencies and experimental results is quantitatively good especially for the $\nu_2$ and $\nu_{27}$ modes in the boat $ET^0$ and flat $ET^+$. Therefore, the scaled frequencies of $\nu_2$ and $\nu_{27}$ of flat $ET^0$ seem to be quantitatively reliable. We will discuss the reliability of this calculation in the next subsections (III-C and D).

**C. Relationship between the Frequency of $\nu_{27}$ and Site Charge.** The optical conductivity spectra $\sigma(\omega)$ shown in Figure 6a were measured with light polarization nearly parallel to the long axis of the ET molecule. The spectra II, III, and IV shown in the figure were measured on the side face of the single crystal which is perpendicular to the conducting sheet. The strong peaks in Figure 6a are located at 1464, 1445, 1400, and 1400 $cm^{-1}$ in the spectra of $\beta''$-$(ET)_2AuBr_2$ (II), $\beta''$-$(ET)_3(HSO_4)_2$ (IV),[31] $(ET)(AuBr_2Cl_2)$ (V), and $(ET)(ClO_4)$ (VI), respectively. These infrared-active strong bands are assigned to the $\nu_{27}$ mode, since they are polarized along the long axis of the ET molecule. Since the $\nu_{27}$ mode appears as a single peak, the site charges, $\rho$, can be regarded as homogeneous within an error of the line width.

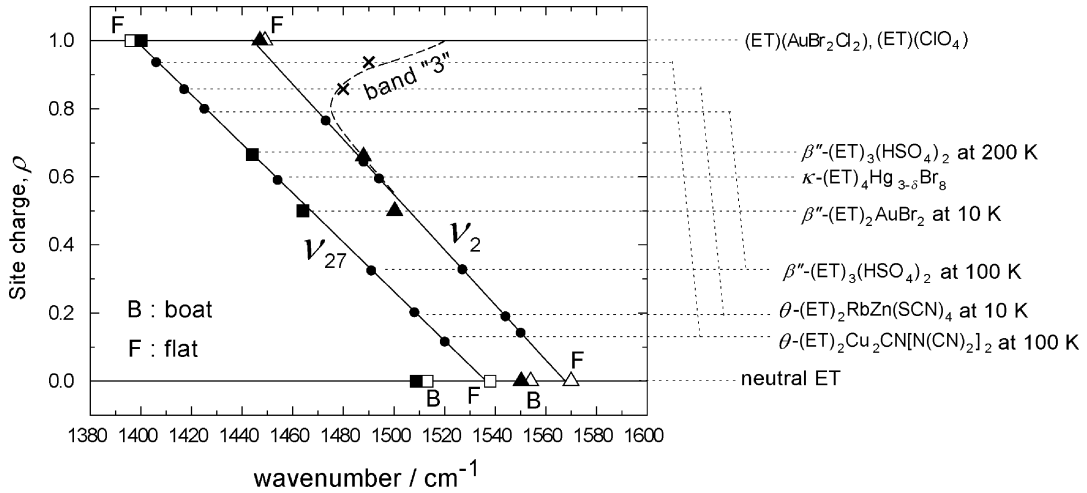


**Figure 7.** Frequencies of the $\nu_{27}$ and $\nu_2$ modes plotted as a function of the charge, $\rho$, on the ET molecule. Solid squares and solid triangles denote the experimental data, and open squares and open triangles denote the calculated data. The straight lines show the linear relationships between the frequencies and $\rho$, deduced from least-squares fitting. The $\rho$ value of the ET salts is inversely estimated from the linear relation, and the data points thus obtained are indicated by solid circles. The broken line shows the $\rho$ dependence of the band "3" (See, section III-D and Figure 8), and $\times$ denotes the frequencies of the *A*-symmetry mode of the $\theta$-type ET salts.

From the chemical compositions, the fractional charges on the molecule are $\rho = +0.5$, $+0.6_6$, $+1$, and $+1$ in II, IV, V, and VI, respectively. The frequency of $\nu_{27}$ is plotted as a function of the corresponding charge in Figure 7. Using the experimentally obtained data (solid squares) and the calculated frequency of the flat $ET^0$ (open square with the letter, "F"), we obtained a straight line for the frequency—$\rho$ plot using least-squares fitting. The linear relationship thus obtained is $\nu_{27}(\rho) = 1398 + 140(1 - \rho)$ cm$^{-1}$. The frequency shift of $\nu_{27}$ between $\rho = 0$ and $+1$ is $\sim$140 cm$^{-1}$, which is much larger than the value of $\sim$60 cm$^{-1}$ reported previously.[17−19] This difference comes from the revised assignment of $\nu_{27}$ of $ET^+$ and the replacement of $\nu_{27}$ of the boat $ET^0$ with that of the flat $ET^0$. We have examined the temperature dependence of the frequency in the $\nu_{27}$ mode using $\beta''$-$(ET)_2AuBr_2$. Since the electrical resistivity exhibits metallic behavior down to the liquid helium temperature, there is no phase transition in $\beta''$-$(ET)_2AuBr_2$. The frequency shift from 300 to 10 K, $\sim +4$ cm$^{-1}$, is comparable to the resolution of the spectrometer, which means that the frequency shift due to the thermal contraction is negligibly small. Therefore, the liner relationship can be applied to the whole temperature range below 300 K. We examined the validity of the linear relationship between $\nu_{27}$ and $\rho$, applying it to several ET salts in a CO state.

First, we examine $\beta''$-$(ET)_3(HSO_4)_2$ in a charge-ordered state at 100 K.[31] The conductivity spectrum of $\beta''$-$(ET)_3(HSO_4)_2$ at 100 K is shown in the bottom panel (IX) of Figure 6b. The two $\nu_{27}$ modes at $\sim$1425 and $\sim$1491 cm$^{-1}$ are assigned based on the polarization and temperature dependence.[31] If we apply the linear relation, $\nu_{27}(\rho) = 1398 + 140(1 - \rho)$ cm$^{-1}$, the fractional charges are estimated to be $\sim +0.8_1$ and $\sim +0.3_4$. According to the X-ray crystal structure analysis, a unit cell contains three ET molecules: two ET molecules in the unit cell are related by the inversion center and one ET molecule is located at the inversion center.[32] If we assume that the unit cell contains two charge-rich molecules and one charge-poor molecule, the total charge in the unit cell is calculated to be $\sim +0.8_1 \times 2 + 0.3_4 \approx +1.9_6$. This value is in excellent agreement with the value of $+2$ expected from the chemical composition. Therefore, we can conclude that the fractional charges in the CO state can be successfully estimated from the linear relationship, including the values of the flat $ET^0$. This conclusion leads to the validity of the calculated frequency of $\nu_{27}$ modes for the flat $ET^0$.

Next, we discuss the spectrum of $\theta$-$(ET)_2Cu_2CN[N(CN)_2]_2$ in a CO state at 100 K (reflectance spectra, VII, in Figure 6b). As described in the preceding section (III-B), the $\nu_{27}$ mode of the charge-poor molecule in $\theta$-$(ET)_2Cu_2CN[N(CN)_2]_2$ is observed at $\sim$1520 cm$^{-1}$. Applying the linear relationship, the fractional charge of the charge-poor molecule is calculated to be $\sim +0.1_2$. There are two bands at $\sim$1406 and 1417 cm$^{-1}$ in the region where the $\nu_{27}$ mode of the charge-rich molecule is expected to appear. One of these two bands corresponds to $\nu_{27}$ of the charge-rich molecule and the other the asymmetric $CH_2$-bending mode. The fractional charge of the charge-rich molecule is calculated to be $\sim +0.9_4$ from $\sim$1406 cm$^{-1}$ and $\sim +0.8_6$ from 1417 cm$^{-1}$. Because the crystal surface was distorted, the absolute value of the reflectivity could not be determined. Nevertheless, we tentatively calculated the optical conductivity from the reflection spectra. In the conductivity spectrum, the $\sim$1406 cm$^{-1}$ band appeared as a main band accompanied by the $\sim$1417 cm$^{-1}$ band as a shoulder. This result suggests that the $\sim$1406 cm$^{-1}$ band is the $\nu_{27}$ mode whereas the $\sim$1417 cm$^{-1}$ band is the $CH_2$-bending mode, which is in agreement with the fact that the $CH_2$-bending mode has a weak intensity in $\beta''$-$(ET)_3(HSO_4)_2$ (see IV and IX in Figure 6). We will discuss this assignment again in the next paragraph. The summation of the fractional charges at the charge-poor and charge-rich molecules is $+1.0_6$ (or $+0.9_8$), which is close to the value of $+1$ expected from the chemical composition. This result also supports the validity of the linear relationship for the $\nu_{27}$ mode.

According to the Raman study of $\theta$-$(ET)_2RbZn(SCN)_4$ in a CO state, the fractional charges of charge-rich and charge-poor molecules are proposed to be $\sim +0.8_5$ and $\sim +0.1_5$.[6] The conductivity spectra of $\theta$-$(ET)_2RbZn(SCN)_4$ in a CO state is shown as plot VIII in Figure 6b. The $\nu_{27}$ mode of the charge-rich molecule is observed at $\sim$1419 cm$^{-1}$, which leads to the estimation of the fractional charge as $\sim +0.8_5$.[33] The $\nu_{27}$ mode of the charge-poor molecule is observed as a weak dip at $\sim$1508 cm$^{-1}$. Accordingly, the fractional charge of the charge-poor molecule is calculated to be $\sim +0.2_1$. The summation of the charges, $\sim +1.0_6$, is also consistent with the chemical

composition. The disproportionation ratio in a CO state is related to the overlap integral between highest occupied molecular orbitals (HOMOs) of the charge-rich and charge-poor molecules: It is accepted that the overlap integral of $\theta$-$(ET)_2$-$RbZn(SCN)_4$ is larger than that of $\theta$-$(ET)_2Cu_2CN[N(CN)_2]_2$.[4,34] Therefore, the disproportionation ratio of $\theta$-$(ET)_2RbZn(SCN)_4$ is expected to be smaller than that of $\theta$-$(ET)_2Cu_2CN[N(CN)_2]_2$. The disproportionation ratio of $\theta$-$(ET)_2RbZn(SCN)_4$ is $[\sim +0.8_5/\sim +0.2_1]$ while that of $\theta$-$(ET)_2Cu_2CN[N(CN)_2]_2$ is $[\sim +0.9_4/\sim +0.1_2]$ or $[\sim +0.8_6/\sim +0.1_2]$. In the latter compound, therefore, $[\sim +0.9_4/\sim +0.1_2]$ seems to be more reasonable than $[\sim +0.8_6/\sim +0.1_2]$. Accordingly, the $\sim$1406 $cm^{-1}$ band is more reasonable as the candidate of the $\nu_{27}$ mode rather than the 1417 $cm^{-1}$ band in the CO state of $\theta$-$(ET)_2Cu_2CN[N(CN)_2]_2$, which is in agreement with the fact that the $\sim$1406 $cm^{-1}$ band appeared as a main band in the conductivity spectra.

The spectrum denoted as III in Figure 6a shows the optical conductivity of $\kappa$-$(ET)_4Hg_{3-\delta}Br_8$ at 300 K. The structure and nonstoichiometric composition of this compound have aroused interest, because this system is regarded as the carrier-doped state in a Mott insulator. The $\nu_{27}$ mode is observed at $\sim$1454 $cm^{-1}$, and the fractional charge is calculated as $\rho \sim +0.6$.[35] This value roughly agrees with the charge of $\rho \sim +0.55$ estimated from $\delta \sim 0.11$, which is deduced from the population analysis of Hg in the X-ray crystal structure analysis.[36]

We can comment briefly on the intensity of the $\nu_{27}$ mode. As shown in Figure 6b, the intensity of the charge-poor molecule is much weaker than that of the charge-rich molecule. Since the $\nu_{27}$ mode is the out-of-phase vibration at the wing C=C bonds, this mode induces an intramolecular charge oscillation between the five-membered rings, which generates a large transition dipole along the molecular long axis.[37] With decreasing $\rho$ down to zero, the net charge decreases, and thus the transition dipole decreases. The enhancement of the transition dipole in $ET^+$ is predicted in the quantum chemical calculation as well.[21]

**D. Relationship between the Frequency of $\nu_2$ and Site Charge.** In this section, we discuss the relationship between the charge on the ET molecule and the frequency of the $\nu_2$ mode. According to the previous Raman studies and this work, the $\nu_2$ modes are observed at 1500, 1488, 1447, and 1447 $cm^{-1}$ in the spectra of $\beta''$-$(ET)_2AuBr_2$ at 50 K,[38] $\beta''$-$(ET)_3(HSO_4)_2$ at 200 K,[31] $(ET)(AuBr_2Cl_2)$ at 300 K, and $(ET)(ClO_4)$ at 300 K, respectively. These experimental data (solid triangles) and the calculated frequency of $ET^0$ (open triangles) are plotted in Figure 7 as a function of the molecular charge, $\rho$. We obtained the least-squares fit using the experimental data for the ET salts and the calculated frequency of the flat $ET^0$ (the open triangle denoted by "F"). The linear relationship between the frequency and charge is given by the equation, $\nu_2(\rho) = 1447 + 120(1 - \rho)$. We can examine the consistency of this equation with the linear relationship for the $\nu_{27}$ mode using the same ET salts as those described in the preceding subsection (III-C). The Raman spectrum of $\beta''$-$(ET)_3(HSO_4)_2$ in a CO state (100 K) exhibits two $\nu_2$ modes, at $\sim$1473 and $\sim$1527 $cm^{-1}$.[31] The respective charges are calculated to be $\sim +0.7_9$ and $\sim +0.3_3$ when applying the linear relationship for $\nu_2$, which are consistent with the charges of $\sim +0.8_1$ and $\sim +0.3_4$ calculated from the linear relationship for $\nu_{27}$. Since the $\nu_2$ mode of $\kappa$-$(ET)_4Hg_{3-\delta}Br_8$ at 300 K is observed at $\sim$1494 $cm^{-1}$, the charge is calculated to be $\sim +0.6$, which is consistent with the value of $\sim +0.6$ estimated from the $\nu_{27}$ mode. In the Raman spectra of $\theta$-$(ET)_2Cu_2CN[N(CN)_2]_2$ and $\theta$-$(ET)_2RbZn(SCN)_4$ salts, the $\nu_2$ mode of the charge-poor molecule appears as a doublet at $\sim$1550 $cm^{-1}$.[4,6] It is reported that the doublet is ascribed to the Fermi resonance between the $\nu_2$ and combination modes.[4,6] We define the frequency of the $\nu_2$ mode of the charge-poor molecule as the average frequency of the doublet. Since the average frequency of $\theta$-$(ET)_2Cu_2CN[N(CN)_2]_2$ and $\theta$-$(ET)_2RbZn(SCN)_4$ is $\sim$1550 and $\sim$1544 $cm^{-1}$, respectively, the charge of the charge-poor molecule is $\sim +0.1_4$ for $\theta$-$(ET)_2Cu_2CN[N(CN)_2]_2$ and $\sim +0.1_9$ for $\theta$-$(ET)_2RbZn(SCN)_4$. These values are also consistent with the charges of $\sim 0.1_2$ for $\theta$-$(ET)_2Cu_2CN[N(CN)_2]_2$ and $\sim +0.2_1$ for $\theta$-$(ET)_2RbZn(SCN)_4$ estimated from the $\nu_{27}$ mode. The data mentioned above are plotted as solid circles in Figure 7. It can be observed that the linear relationship for the $\nu_2$ mode is consistent with the relationship for the $\nu_{27}$ mode.

However, the linear relationship for the $\nu_2$ mode cannot be applied to the charge-rich molecule of $\theta$-$(ET)_2Cu_2CN[N(CN)_2]_2$ and $\theta$-$(ET)_2RbZn(SCN)_4$. When the linear relation of $\nu_{27}$ is applied, the fractional charge of the charge-rich molecules in $\theta$-$(ET)_2Cu_2CN[N(CN)_2]_2$ and $\theta$-$(ET)_2RbZn(SCN)_4$ is estimated to be $\sim +0.9_4$ and $\sim +0.8_5$, respectively, as discussed in the preceding section (III-C). If we calculate the frequency of the $\nu_2$ mode of the charge-rich molecule using the linear relationship for the $\nu_2$ mode, then the $\nu_2$ modes are calculated to appear at $\sim$1454 and $\sim$1465 $cm^{-1}$, respectively. The observed Raman bands closest to these calculated values are the $\sim$1450 and $\sim$1455 $cm^{-1}$ bands, respectively.[4,6] However, such bands are assigned to $\nu_3$ based on the isotope shift of $\theta$-$(^{13}C\text{-}ET)_2$-$RbZn(SCN)_4$.[6] The next closest band is observed at $\sim$1480 $cm^{-1}$ for $\theta$-$(ET)_2RbZn(SCN)_4$,[39] which is assigned to $\nu_2$ of the charge-rich molecule based on the isotope shift experiment.[6] The corresponding band for $\theta$-$(ET)_2Cu_2CN[N(CN)_2]_2$ is observed at $\sim$1490 $cm^{-1}$.[39] These frequencies are significantly higher than the frequency expected from the linear relationship for the $\nu_2$ mode. It should be noted that the deviations are not ascribed to the nonplaner structure since the ET molecules in the CO state keep the flat structure.[14]

The deviation from the linear relationship for $\nu_2$ can be ascribed to the interaction with the $\nu_3$ mode. As described in previous reports,[4,6,7] the splitting of the $\nu_3$ mode in a CO state is determined mainly by the e-mv interaction rather than by the fractional charge. As shown in Figure 1, the charge-rich molecule is adjacent to the charge-poor molecule. Since the $\nu_3$ mode at the charge-poor molecule interacts with that at the charge-rich molecule, the highest frequency mode decreases to the frequency of the average charge between the charge-rich and charge-poor molecules, +0.5.[4,7] The frequency of the corresponding mode is then estimated to be $\sim$1465 $cm^{-1}$.[40] This frequency is close to the frequency of $\nu_2$ at the charge-rich molecule, which is expected from the linear relationship. Therefore, the interaction between $\nu_3$ and $\nu_2$ splits these two modes: The $\sim$1450 and $\sim$1490 $cm^{-1}$ ($\sim$1455 and $\sim$1480 $cm^{-1}$) bands correspond to the hybridized modes between $\nu_3$ and $\nu_2$ in $\theta$-$(ET)_2Cu_2CN[N(CN)_2]_2$ ($\theta$-$(ET)_2RbZn(SCN)_4$).[4,6]

To verify the hybridization between $\nu_2$ and $\nu_3$ through intermolecular interactions, we calculated the site-charge dependence of the frequency of the vibronic modes using the asymmetric tetramer model,[4,7] which is effective for the determination of the splitting of the vibronic mode in a charge-ordered state. The tetramers shown in the corners of Figure 8a are the repeating units of the "horizontal stripe" in Figure 1. The detailed procedure of the nonhybrid case is described in refs 4 and 7, where the vibronic $\nu_3$ mode is treated independently

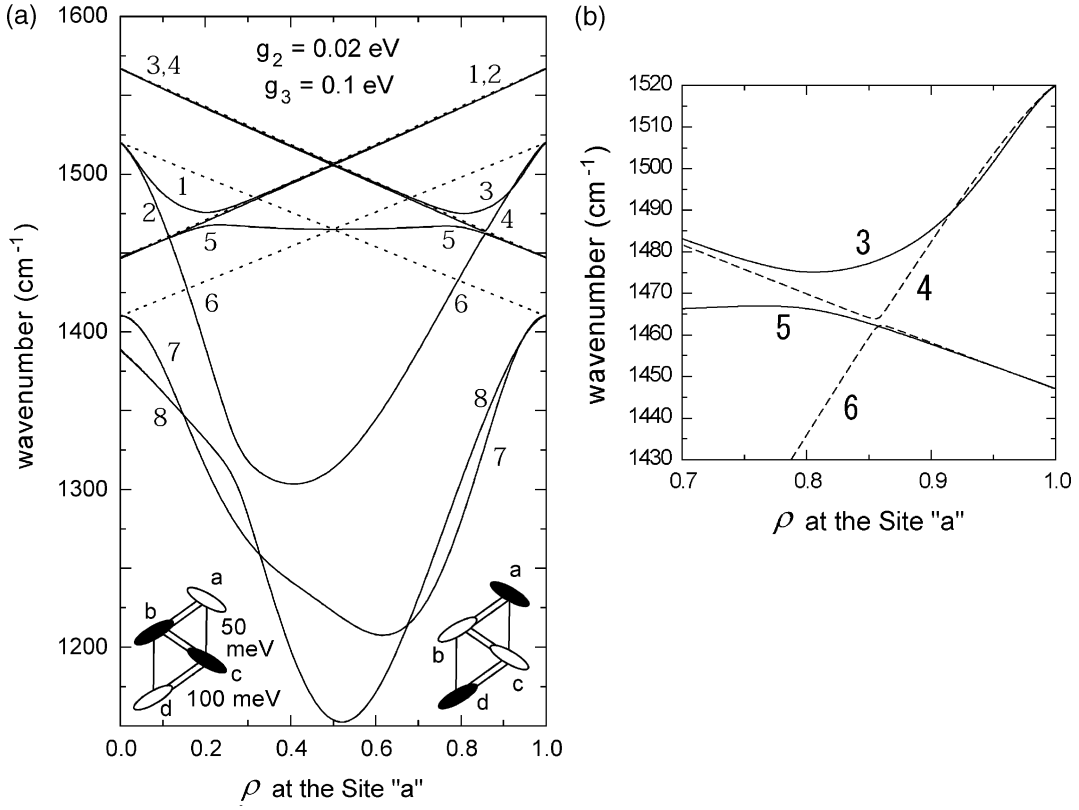


**Figure 8.** (a) Frequencies of the vibronic bands of the $\nu_3$ and $\nu_2$ modes plotted against the molecular charge at the site "a", $\rho_a$. Dotted lines show the unperturbed frequencies of the $\nu_3$ and $\nu_2$ modes. Schematic views of the nonlinear tetramer are shown at the corners of the figure. The nonliner tetramer is extracted from the "horizontal CO state" in Figure 1. A gray ellipse denotes the charge-rich site. The double and single lines in the tetramer denote the magnitudes of the transfer integrals. (b) Expanded figure of the bands 3−6 in the region where hybridization occurs between $\nu_3$ and $\nu_2$.

of the $\nu_2$ mode. To avoid redundancy, the detailed procedure is omitted in the presented paper. We modified the Hamiltonian given in the literature[4,7] to calculate the $\nu_2$ and $\nu_3$ modes simultaneously. The Hamiltonian is modified as follows ($\hbar = 1$)

$$H = H_e + H_v + H_{ev} \tag{1}$$

$$H_e = \sum_{i=1}^{4}\Delta_i n_i + \sum_{\sigma}\sum_{i\neq j}^{4} t_{ij}(c_{i\sigma}{}^{+}c_{j\sigma} + c_{j\sigma}{}^{+}c_{i\sigma}) + U\sum_{i=1}^{4} n_{i\uparrow}n_{i\downarrow} + \sum_{i\neq j}^{4} V_{ij}n_i n_j \tag{1-1}$$

$$H_v = \frac{1}{2}\sum_{v=2}^{3}\sum_{i}^{4}(P_{v,i}{}^2 + Q_{v,i}{}^2\omega_{v,i}{}^2) \tag{1-2}$$

$$H_{ev} = \sum_{v=2}^{3} g_v \sum_{i=1}^{4} n_i\sqrt{2\omega_{v,i}}Q_{v,i} \tag{1-3}$$

where $i$ and $j$ denote the site number (a−d molecules in Figure 8a), $t_{ij}$ is the transfer integral between sites $i$ and $j$, $c_i^+$ ($c_i$) is the creation (annihilation) operator with $\sigma$ spin, $\Delta_i$ is the site energy, and $U$ is the on-site Coulombic energy. The number operator is $n_i = c_i^+c_i$ at the $i$th site, and the summation over four sites, $\sum_{i=1}^{4}\langle n_i\rangle = 2$, corresponds to the total number of holes within the tetramer. $V_{ij}$ is the intersite Coulombic energy between site $i$ and site $j$. $P_{v,i}$ and $Q_{v,i}$, respectively, denote the momentum operator and the normal coordinate of the $v$th mode ($\nu_2$ and $\nu_3$ modes) at site $i$, and $g_v$ is the e-mv coupling constant of the $v$th mode (∼0.02 eV for $v = 2$ and ∼0.1 eV for $v = 3$).[19] The $\omega_{v,i}$ value is the unperturbed vibrational frequency of the $v$th mode at the $i$th site, which is assumed to be $\omega_{v,i} = \omega_{v,N}(1 - \rho_i) + \omega_{v,I}\rho_i$, where $\omega_{2,N} = 1567$ cm$^{-1}$, $\omega_{2,I} = 1447$ cm$^{-1}$, $\omega_{3,N} = 1520$ cm$^{-1}$, and $\omega_{3,I} = 1410$ cm$^{-1}$ are the frequencies of the $\nu_2$ and $\nu_3$ modes for the neutral and ionic ET molecules. The $Q$-dependent ground-state energy is obtained using the perturbation method

$$E(Q) = E_1 + \langle\Psi_1|H_{ev}(Q)|\Psi_1\rangle + \sum_{m=2}^{16}\frac{|\langle\Psi_1|H_{ev}(Q)|\Psi_m\rangle|^2}{E_1 - E_m} \tag{2}$$

where $E_m$ denotes the energy of the electronic excited states and $\Psi_m$ is the corresponding wave function. Unperturbed electronic states are solved by exact diagonalization. The perturbed frequencies are numerically calculated by constructing the force-constants matrix from the second derivative of $E(Q)$ by $Q_{v,i}$.[41] The force-constants matrix contains the cross terms, for example $\partial E/\partial Q_{2,1}\partial Q_{3,2}$, which are not incorporated in the previous models.[4,7] The cross terms contribute to the interaction between the $\nu_2$ mode at the charge-rich (poor) molecule and the $\nu_3$ mode at the charge-poor (rich) molecule. Since the tetramer contains four ET molecules, four $\nu_2$ modes and four $\nu_3$ modes participate in the interactions. Therefore, the frequencies of eight eigenmodes are deduced. The site charge, $\rho_i$, is calculated using the following equation

$$\rho_i = \langle\Psi_1|n_i|\Psi_1\rangle \tag{3}$$

$t_{ij}$, $U$, and $V$ are treated as the fixed values, $t_{12} = t_{24} = t_{34} = 2t_{14} = 2t_{23} = 100$ meV, $U = 0.8$ eV, and $V_{12} = V_{24} = V_{34} =$

$V_{23} = V_{14} = 0.33$ eV, to compare the nonhybrid model by Suzuki et al.[7] (see ref 42). The repeating unit of the horizontal stripe, shown in the corners of Figure 8a, is reproduced when the site energy, $\Delta_i$, is treated as a variable.

Figure 8a shows the $\rho_a$ (molecular charge at site "a") dependence of the eight vibrational modes thus obtained. Since the screw axis runs along the crystallographic *a*-axis (Figure 1), the eight eigenmodes, 1−8, are classified into the *A*- and *B*-symmetry. The odd and even numbers correspond to the *A*- and *B*-symmetry, respectively. By the comparison of Figure 8a with Figure 12 in ref 7, the frequencies of the eight modes are almost identical to those of the nonhybrid model within the range of $0.2 \leq \rho_a \leq 0.8$. In this range, the modes 1−4 correspond to the vibronic $\nu_2$ modes, the modes 5−8 correspond to the vibronic $\nu_3$ modes, and the vibronic $\nu_2$ modes are almost independent of the vibronic $\nu_3$ modes.

Next, we discuss the behavior of each mode above $\rho_a \sim 0.8$ or below $\rho_a \sim 0.2$. The behavior of the modes 1, 2, 8, and 7 above $\rho_a \sim 0.8$ (3, 4, 8, and 7 below $\rho_a \sim 0.2$) is almost identical to the nonhybrid case. The $\nu_2$ mode at the charge-poor molecules mostly contributes to the modes 1 and 2 above $\rho_a \sim 0.8$ (3 and 4 below $\rho_a \sim 0.2$), while the modes 8 and 7 are mostly the vibronic $\nu_3$ modes. Therefore, the charge at the charge-poor molecule can be safely estimated from the linear relationship of the $\nu_2$ mode. On the contrary, the modes 3−6 (1, 2, 5, and 6) exhibit a complicated behavior in the regions of $\rho_a \geq 0.8$ ($\rho_a \leq 0.2$). Since the $\rho_a$ dependence below $\rho_a \sim 0.2$ is the mirror image of the $\rho_a$ dependence above $\rho_a \sim 0.8$, we discuss the behavior of the modes 3−6 above $\rho_a \sim 0.8$. As shown in Figure 8b, the *A*-modes denoted as 3 and 5 are separated from each other owing to the hybridization of $\nu_2$ and $\nu_3$. With an increase in $\rho_a$ up to ~1, the frequency of the mode 3 drastically increases, since the contribution of $\nu_3$ to the mode 3 rapidly increases. The charge at the charge-rich molecule of $\theta$-$(ET)_2Cu_2CN[N(CN)_2]_2$ is more positive than that of $\theta$-$(ET)_2RbZn(SCN)_4$ according to the estimation from the $\nu_{27}$ mode (see section III-C). Therefore, the behavior in the mode 3 explains the observation that the *A*-symmetry band (~1490 $cm^{-1}$) of the former is higher than that (~1480 $cm^{-1}$) of the latter, which is shown as the broken line in Figure 7.

The *B*-symmetry modes 4 and 6 also exhibit hybridization at $\rho_a \sim 0.8$[5]. In contrast to the *A*-symmetry modes, however, the separation between 4 and 6 bands is negligible. Therefore, the frequency of mode 4 is lower than that of mode 3. This result explains the polarization dependence of the Raman spectra of $\theta$-$(ET)_2Cu_2CN[N(CN)_2]_2$: the frequency of the *B*-symmetry band, ~1480 $cm^{-1}$, is lower than that of the *A*-symmetry band, ~1490 $cm^{-1}$ (see Figure 3b in ref 4). Therefore, we have concluded that the hybridization between $\nu_2$ and $\nu_3$ in the CO state is responsible for the deviation from the linear relationship for the $\nu_2$ mode. On the other hand, such an interaction is negligible when the difference in the site charges, $\Delta\rho$, is not so large since the $\nu_2$ mode is well separated from the $\nu_3$ mode.

In summary, we have determined the frequency of the $\nu_{27}$ mode of $ET^+$ from the reflectance spectra of $(ET)(ClO_4)$ and $(ET)(AuBr_2Cl_2)$. According to the DFT calculations, the frequency of the $\nu_{27}$ mode of $ET^0$ is sensitive to the molecular structure—the frequency of the flat $ET^0$ molecule is higher by 25 $cm^{-1}$ than that of the boat $ET^0$ molecule. This calculation explains the apparent unreasonable result that the charge-poor ET molecule has a negative charge in the charge-ordered state of $\theta$-$(ET)_2Cu_2CN[N(CN)_2]_2$. Combining the experimental data with the calculated results, we obtained the linear relationships between the frequencies and the molecular charge, $\rho$. The equations were determined to be $\nu_{27}(\rho) = 1398 + 140(1 - \rho)$ $cm^{-1}$ for the $\nu_{27}$ mode and $\nu_2(\rho) = 1447 + 120(1 - \rho)$ $cm^{-1}$ for the $\nu_2$ mode. The linear relationship of the $\nu_2$ mode cannot be applied to the charge-rich molecules of the $\theta$-type ET salts because the $\nu_2$ and $\nu_3$ modes are hybridized in the charge-ordering state. On the other hand, the linear relationship of the $\nu_{27}$ mode ET is applicable in the whole range of $0 \leq \rho \leq 1$, because $\nu_{27}$ is free from e-mv interactions and isolated from other normal modes of ET. Therefore, the $\nu_{27}$ mode is the most reliable probe for the estimation of the site charges.

**Acknowledgment.** This work was partly supported by a Grant-in-Aid for Scientific Research on Priority Areas of Molecular Conductors (No. 15073223) from the Ministry of Education, Culture, Sports, Science and Technology, Japan.

## References and Notes

(1) For example see: (a) Highly Conducting quasi one-dimensional Organic Crystals. In *Semiconductors and Semimetals*; Conwell, E., Ed.; Academic Press: London, 1988; Vol. 27. (b) Graja, A. *Low dimensional Organic Conductors*; World Scientific Publishing: Singapore, 1992.

(2) Structural data of the numerical CT salts containing ET are described in: (a) Mori, T. *Bull. Chem. Soc. Jpn*. **1998**, *71*, 2509. (b) Mori, T. *Bull. Chem. Soc. Jpn*. **1999**, *72*, 2011. (c) Mori, T.; Mori, H.; Tanaka, S. *Bull. Chem. Soc. Jpn*. **1999**, *72*, 179.

(3) Yamamoto, T.; Uruichi, M.; Yakushi, K.; Yamaura, J.; Tajima, H. *Phys. Rev. B* **2004**, *70*, 125102.

(4) Yamamoto, T.; Yakushi, K.; Shimizu, H.; Saito, G. *J. Phys. Soc. Jpn.* **2004**, *73*, 2326.

(5) Wojciechowski, R.; Yamamoto, K.; Yakushi, K.; Kawamoto, A. *Phys. Rev. B* **2003**, *67*, 224105.

(6) Yamamoto, K.; Yakushi, K.; Miyagawa, K.; Kanoda, K.; Kawamoto, A. *Phys. Rev. B* **2002**, *65*, 085110.

(7) Suzuki, K.; Yamamoto, K.; Yakushi, K. *Phys. Rev. B* **2004**, *69*, 085114.

(8) As described in the previous literature,[4,6,7] the horizontal stripe includes the 1-D stripe which consists of either a charge-rich molecule or a charge-poor molecule extending along the crystallographic *a*-axis. The 1-D stripes are stacked along the crystallographic *c*-axis, so that a charge-rich stripe is sandwiched by charge-poor stripes.

(9) Merino, J.; McKenzie, R. H. *Phys. Rev. Lett.* **2001**, *87*, 237002.

(10) Akutsu, H.; Sato, A. A.; Turner, S. S.; Le Pevelen, D.; Day, P.; Laukhin, V.; Klehe, A.-K.; Singleton, J.; Tocher, D. A.; Probert, M. R.; Howard, J. A. K. *J. Am. Chem. Soc.* **2002**, *124*, 12430.

(11) Nad, F.; Monceau, P.; Carcel, C.; Fabre, J. M. *Phys. Rev. B* **2000**, *62*, 1753.

(12) Chiba, R.; Hiraki, K.; Takahashi, T.; Yamamoto, H. M.; Nakamura, T. *Phys. Rev. Lett.* **2004**, *93*, 216405.

(13) Miyagawa, K.; Kawamoto, A.; Kanoda, K. *Phys. Rev. B* **2000**, *62*, R7679.

(14) Watanabe, M.; Noda, Y.; Nogami, Y.; Mori, H. *J. Phys. Soc. Jpn.* **2004**, *73*, 116.

(15) Wang, H. H.; Ferraro, J. R.; Williams, J. M.; Geiser, U.; Schlueter, J. A. *J. Chem. Soc. Chem. Commun.* **1994**, 1893. In this reference, $\nu_2$ is designated as $\nu_3$.

(16) The Raman-active mode $\nu_3$, which is the stretching mode of the central C═C bond, is influenced by the e-mv interaction much more than charge difference.

(17) Moldenhauer, J.; Horn, Ch.; Pokhodnia, K. I.; Schweitzer, D.; Heinen, I.; Keller, H. J. *Synth. Met*. **1993**, *60*, 31.

(18) Kozlov, M. E.; Pokhodnia, K. I.; Yurchenko, A. A. *Spectrochim. Acta* **1987**, *43A*, 323.

(19) Kozlov, M. E.; Pokhodnia, K. I.; Yurchenko, A. A. *Spectrochim. Acta* **1989**, *45A*, 437.

(20) Eldridge, J. E.; Homes, C. C.; Williams, J. M.; Kini, A. M.; Wang, H. H. *Spectrochim. Acta* **1995**, *51A*, 947.

(21) Demiralp, E.; Dasgupta, S.; Goddard, W. A., III. *J. Phys. Chem.* **1997**, *101*, 1975.

(22) Kobayashi, H.; Kobayashi, A.; Sasaki, Y.; Saito, G.; Inokuchi, H. *Bull. Chem. Soc. Jpn.* **1986**, *59*, 301.

(23) This method enables us to exclude $\beta''$-$(ET)_2(ClO_4)$TCE from the products.

(24) Abboud, K. A.; Chou, L. K.; Clevenger, M. B.; de Oliveira, G. F.; Talham, D. R. *Acta Crystallogr.* **1995**, *C51*, 2356.

(25) Porter, L. C.; Wang, H. H.; Beno, M. A.; Carlson, K. D.; Pipan, C. M.; Proksch, R. B.; Williams, J. M. *Solid State Commun.* **1987**, *64*, 387.

(26) *GAUSSIAN98*, revision A.11; Gaussian, Inc.

(27) Becke, A. D. *J. Chem. Phys.* **1992**, *97*, 9173. Lee, C.; Yang, W.; Parr, R. G. *Phys. Rev. B* **1988**, *37*, 785.

(28) We also measured the spectra with the incident lights polarized along the stacking directions (corresponding to the *c*- and *a*-directions for $ClO_4$ and $AuBr_2Cl_2$ salts, respectively). These spectral shapes are almost the same as those shown in Figure 4 except for the intensities.

(29) The same result has been already reported by Kozlov et al. in ref 18.

(30) Scott, A. P.; Radom, L. *J. Phys. Chem.* **1996**, *100*, 16502.

(31) Yamamoto, T.; Uruichi, M.; Yakushi, K.; Kawamoto, A. Unpublished work. The $\nu_{27}$ mode is observed as a single peak above the metal−insulator transition temperature, but two bands appeared abruptly just below the transition temperature. However, the frequency of the $\nu_{27}$ mode above the phase-transition temperature shows weak temperature dependence, although the ET molecules have a planar structure. We consider that the charge at 300 K is slightly deviated from the averaged value, $+0.6_7$. Therefore, we adopted the 200 K spectrum as a standard frequency for $+0.6_7$ since the $\nu_{27}$ mode at 200 K has a narrower line width. The $\nu_2$ mode also exhibits the same temperature dependence.

(32) Miyazaki, A.; Enoki, T.; Uekusa, H.; Ohashi, U. *Phys. Rev. B* **1997**, *55*, 6847.

(33) As shown in Figure 5b-VIII, the ∼1419 $cm^{-1}$ band has a shoulder at ∼1414 $cm^{-1}$. This shoulder is assignable to the $CH_2$-bending mode.

(34) Mori, H.; Tanaka, S.; Mori, T. *Phys. Rev. B* **1998**, *57*, 12023.

(35) The line width of $\kappa$-$(ET)_4Hg_{3-\delta}Br_8$ at 300 K is ∼26 $cm^{-1}$, which is significantly wider than that of the spectral resolution, 4 $cm^{-1}$. This observation suggests inhomogeneous charge distributions.

(36) Lyubovskaya, R. N.; Zhilyaeva, E. I.; Pesotskii, S. I.; Lyubovskii, R. B.; Atovmyan, L. O.; D'yachenko, O. A.; Takhirov, T. G. *JETP Lett.* **1987**, *46*, 188.

(37) (a) Swietlik, R.; Kushch, N. D.; Kushch, L. A.; Yagubskii, E. B. *Phys. Status Solidi B* **1994**, *181*, 499. (b) Swietlik, R.; Lagrange, C. G. *Synth. Met.* **1993**, *55*, 2217.

(38) We have examined the temperature dependence of the frequency in the $\nu_2$ mode using $\beta''$-$(ET)_2AuBr_2$. The frequency shift from 300 to 50 K, ∼2 $cm^{-1}$, is comparable to the resolution of the spectrometer. Therefore, the frequency shift due to the thermal contraction is negligibly small.

(39) The ∼1480 $cm^{-1}$ band and the ∼1490 $cm^{-1}$ band are designated as the $\mathbf{a}_2$ band in ref 6 and the ×3 band in ref 4, respectively.

(40) The frequency of the $\nu_3$ mode at $\rho = 0.5$ is estimated to be ∼1465 $cm^{-1}$ on the basis of our results, that is ∼1410 $cm^{-1}$ for $\rho = +1$ and ∼1520 $cm^{-1}$ for $\rho = 0$.

(41) Paineli, A.; Girlando, A. *J. Chem. Phys.* **1986**, *84*, 5655.

(42) The parameters by Suzuki et al.[7] differ from those by Yamamoto et al.,[4] where $V_{ij}$, anisotropic and $t_{ij}$, anisotropic and variable. However, there is no serious difference in both results, except for the two vibronic $\nu_3$ bands, which are mostly perturbed by the e-mv interaction and the frequencies are lower than unperturbed frequency of $ET^+$ (bands 7 and 8 in Figure 8a).